npj | systems biology and applications

www.nature.com/npjsba

ARTICLE OPEN

Check for updates

Optimal energy and redox metabolism in the cyanobacterium *Synechocystis* sp. PCC 6803

Amit Kugler[1] and Karin Stensjö[1]✉

Understanding energy and redox homeostasis and carbon partitioning is crucial for systems metabolic engineering of cell factories. Carbon metabolism alone cannot achieve maximal accumulation of metabolites in production hosts, since an efficient production of target molecules requires energy and redox balance, in addition to carbon flow. The interplay between cofactor regeneration and heterologous production in photosynthetic microorganisms is not fully explored. To investigate the optimality of energy and redox metabolism, while overproducing alkenes—isobutene, isoprene, ethylene and 1-undecene, in the cyanobacterium *Synechocystis* sp. PCC 6803, we applied stoichiometric metabolic modelling. Our network-wide analysis indicates that the rate of NAD(P)H regeneration, rather than of ATP, controls ATP/NADPH ratio, and thereby bioproduction. The simulation also implies that energy and redox balance is interconnected with carbon and nitrogen metabolism. Furthermore, we show that an auxiliary pathway, composed of serine, one-carbon and glycine metabolism, supports cellular redox homeostasis and ATP cycling. The study revealed non-intuitive metabolic pathways required to enhance alkene production, which are mainly driven by a few key reactions carrying a high flux. We envision that the presented comparative in-silico metabolic analysis will guide the rational design of *Synechocystis* as a photobiological production platform of target chemicals.

npj Systems Biology and Applications (2023)9:47 ; https://doi.org/10.1038/s41540-023-00307-3

INTRODUCTION

Cyanobacteria are photosynthetic microbes that serve as an attractive platform for the sustainable production of chemicals and fuels, mainly due to their capability of converting atmospheric carbon dioxide into organic compounds by using solar energy, their relative rapid growth rate, and the readily available genetic toolbox for various species[1]. In the past years, the unicellular cyanobacterium *Synechocystis* sp. PCC 6803 (hereafter *Synechocystis*) has been successfully used as a cell factory for the production of commodity chemicals, including, *n*-butanol[2], bisabolene[3] and phenylpropanoids[4]. Besides autotrophy, cyanobacteria are able to grow under mixotrophic conditions. Mixotrophic metabolism allows the cells to catabolize organic carbon parallel to CO_2 being assimilated photosynthetically. Addition of organic substrates in light growth conditions, though increasing the risk of contamination and cost, is considered as a promising cultivation strategy for the commercialization of cyanobacteria[5,6], owing to enhanced biomass[7] and chemical yield[8,9].

The biosynthesis of various cell metabolites involves biochemical reactions, which require cofactors, such as adenosine triphosphate (ATP) and reduced nicotinamide adenine dinucleotides [NAD(P)H]. ATP is the major energy carrier in the cell, driving numerous metabolic pathways. The pyridine nucleotides NADH and NADPH serve as reducing equivalents in redox reactions. While NADH participates mainly in catabolic reactions, NADPH plays a role in anabolic reactions. In cyanobacteria, the photosynthetic electron transport chain is the major source for ATP and NADPH generation, when grown under light conditions[10]. The different glycolytic routes and the TCA cycle generate reducing agent in the form of NADH. In addition, transhydrogenases catalyze the interconversion between NADH and NADPH[11].

Optimal performance of photosynthesis requires that the light-energy conversion by the photosystems and the downstream metabolic pathways are fine-tuned, to support the ATP/NADPH output ratio and the cellular energy economy[12]. The photosynthetic linear electron flow (LEF) in *Synechocystis* generates an ATP/NADPH ratio of approximately 1.28, which is less than required for CO_2 fixation by the Calvin–Benson–Bassham (CBB) cycle and downstream biochemical pathways[12]. To deal with this imbalance, alternative pathways contributing to ATP production exist[13,14]. In addition, re-oxidation of NAD(P)H to $NAD(P)^+$ and phosphorylation-dephosphorylation of reducing equivalents are important for balancing the ATP/NADPH budget and maintaining redox homeostasis[15]. Despite the importance of meeting the energy and redox requirement to achieve an efficient cellular performance[16,17], only few metabolic engineering efforts of *Synechocystis* have targeted this designing strategy[18], while most studies are concerned with controlling carbon partitioning[1].

Constraint-based modelling (CBM) has been employed for the characterization of physiological capabilities of *Synechocystis*, for which several detailed genome-scale metabolic reconstructions are available[19–25]. CBM is based on imposing of a set of constraints that govern the operation of a metabolic network at steady state. These include, for example, the stoichiometry of the biochemical reactions, mass balance and thermodynamic laws. Flux balance analysis (FBA) is a common CBM-based approach to calculate, under given constraints, the intracellular flux distributions within the stoichiometric network, by optimizing an objective function[26]. As such, FBA can be used to predict the maximum (or minimum) growth rate or the production of desired metabolites, as well as to identify genetic interventions that force carbon flux toward chosen compound. Case studies demonstrating model-driven metabolic engineering of *Synechocystis* include the overproduction production of isoprene[27], *n*-butanol[28] and ethanol[29].

In this work, we focus on alkenes, commercially valuable platform chemicals, which are traditionally used as detergents, lubricants and rubbers. In addition, they are compatible hydrocarbon fuels, due to their high energy content[30]. The development

[1]Microbial Chemistry, Department of Chemistry-Ångström Laboratory, Uppsala University, Box 523, SE-751 20 Uppsala, Sweden. ✉email: karin.stensjo@kemi.uu.se

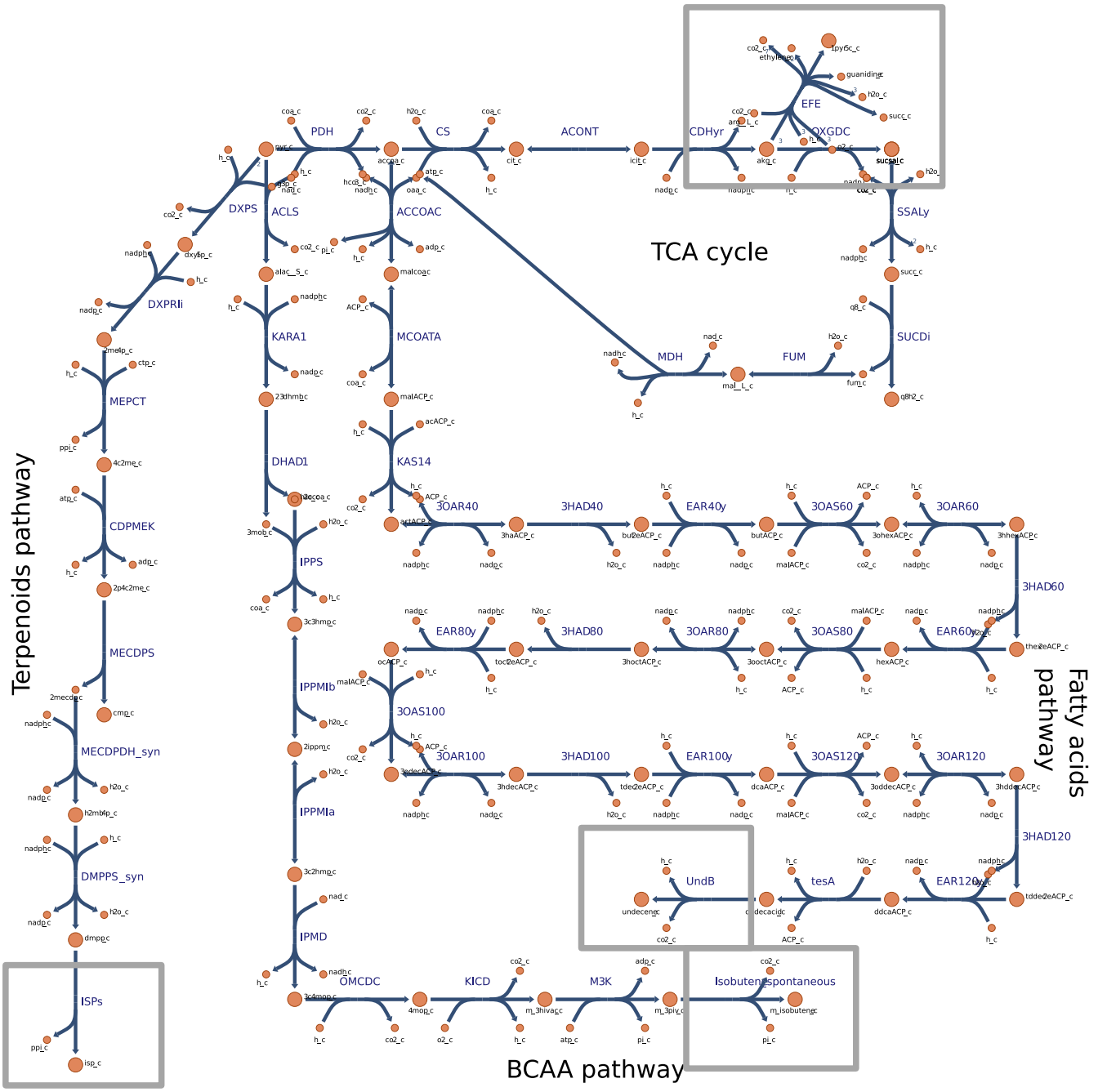

Fig. 1 Non-native alkene biosynthesis pathways reconstructed in the iJN678_AK *Synechocystis* sp. PCC 6803 genome-scale model for cofactor balance analysis. TCA tricarboxylic acid, BCAA branched-chain amino acids. Irreversible reactions are indicated by one-headed arrows; reversible reactions are indicated by two-headed arrows. Metabolic reactions and metabolites (except heterologous ones) are indicated by their BiGG identifier[73].

of gas-to-liquid technologies, enabling the oligomerization of small gaseous substrates into liquid chemicals, together with the environmental concerns associated with the use of fossil fuels and carbon dioxide emissions[31], are driving the necessity for an environmentally-friendly, yet economically-feasible, manufacturing process of bio-alkenes[32,33].

We addressed the question of how the model cyanobacterium *Synechocystis* balances its anabolic-catabolic processes, with respect to central cofactor metabolites [ATP and NAD(P)H], during growth under autotrophic and mixotrophic conditions. To this end, we employed genome-scale metabolic modelling, and analyzed the metabolism of *Synechocystis* strains overproducing alkenes as a case study.

RESULTS AND DISCUSSION

To enable a system analysis of alkene-overproducing *Synechocystis* strains, and assess the resulting energy and redox (im)balance, we chose four alkenes whose production using cyanobacteria has been previously demonstrated: isoprene[34], isobutene[35], ethylene[36] and 1-undecene[37]. The four alkenes stem from different metabolic routes and possess different cofactors requirements (Fig. 1, Table 1).

Evaluation of maximal production capability

First, we examined how increasing growth rate affected alkene production, using phenotypic phase plane analysis[38]. Under both autotrophic and mixotrophic growth conditions, we noticed a trade-off between growth (biomass production) and product synthesis. Predicted maximal alkene production rates resulted in zero biomass accumulation, and vice-versa (Fig. 2a–d). Therefore, we aimed to simulate a more real scenario, in which a cell produces high amounts of alkenes, whilst sustaining minimal biomass synthesis (Fig. 3a). We performed the computational analysis in a two-step optimization strategy (see Methods section).

Subsequently, we evaluated the theoretical maximum production capability, by analyzing the maximum productivity, maximum mass yield and maximum c-mol yield (Table 2); all are parameters of interest from both biotechnological and biochemical aspects. By comparing carbon-source-dependent bioproduction, our computational analysis illustrated that the maximum theoretical mass yield is approximately doubled under mixotrophic conditions, as compared to autotrophic condition, for the production of the examined alkenes. Except for 1-undecene, autotrophic conditions resulted in a comparable productivity for all objectives. Under both growth conditions, the yields were similar for all alkenes, except for ethylene, for which these values were lower. Under autotrophic growth, the release rate of CO_2 is 3.81 mmol/gDW/h for biomass production, whereas ethylene production resulted in a release rate of 5.27 mmol/gDW/h (Supplementary Table 6). Thus, the low yields found for ethylene can be owed to the high carbon loss.

Table 1. Evaluated turnover rates of energy and redox carriers.

	ATP		NADPH		NADH		ATP/NADPH	
Objective	Auto	Mixo	Auto	Mixo	Auto	Mixo	Auto	Mixo
Biomass	8.15	5.35	3.87	0.28	0.12	0.07	2.11	19.49
Isoprene	8.36	5.25	5.09	0.93	0.01	0.01	1.64	5.67
Isobutene	8.61	5.81	5.47	1.85	0.35	0.26	1.57	3.15
Ethylene	7.67	6.82	4.26	2.68	0.49	0.55	1.80	2.55
1-undecene	7.24	5.38	5.49	1.19	0.01	0.01	1.32	4.51

Synechocystis was simulated to grow autotrophically and mixotrophically, when maximizing biomass and alkenes production. For each end-product, the ATP, NADPH and NADH turnover rates and the corresponding ATP/NADPH ratios were computed.
Auto autotrophic, *Mixo* mixotrophic.

Evaluation of ATP and NAD(P)H demands

We then analyzed *Synechocystis* metabolism from the metabolite-centric point of view, also termed as flux-sum analysis[39]. This approach is useful for understanding metabolite essentiality[40], and for studying the intracellular network robustness to perturbations in metabolite turnover rates[39]. Even though the net accumulation of a metabolite might be zero, the overall turnover rate is an indicator of the importance of the specific metabolite.

Under both autotrophic and mixotrophic growth, a higher usage of NADPH (turnover rate of 3.87–5.49 mmol/gDW/h), and ATP (turnover rate of 7.24–8.61 mmol/gDW/h) was observed, as compare to the usage of NADH (turnover rate of 0.01–0.49 mmol/gDW/h) (Table 1). These results are in line with previous experimental studies, showing that NADPH is being preferentially used over NADH in *Synechocystis*, when grown under autotrophic conditions[10]. In addition, all strains exhibited a comparable ATP requirement, although with some variations. For example, less ATP was required for 1-undecene production under autotrophic conditions, and for isoprene under mixotrophic conditions. Under mixotrophic conditions, lower turnover rates were observed for both NADPH and NADH. An explanation for these observations is that the introduced biosynthesis pathways are mainly anabolic, and therefore use more NADPH than NADH.

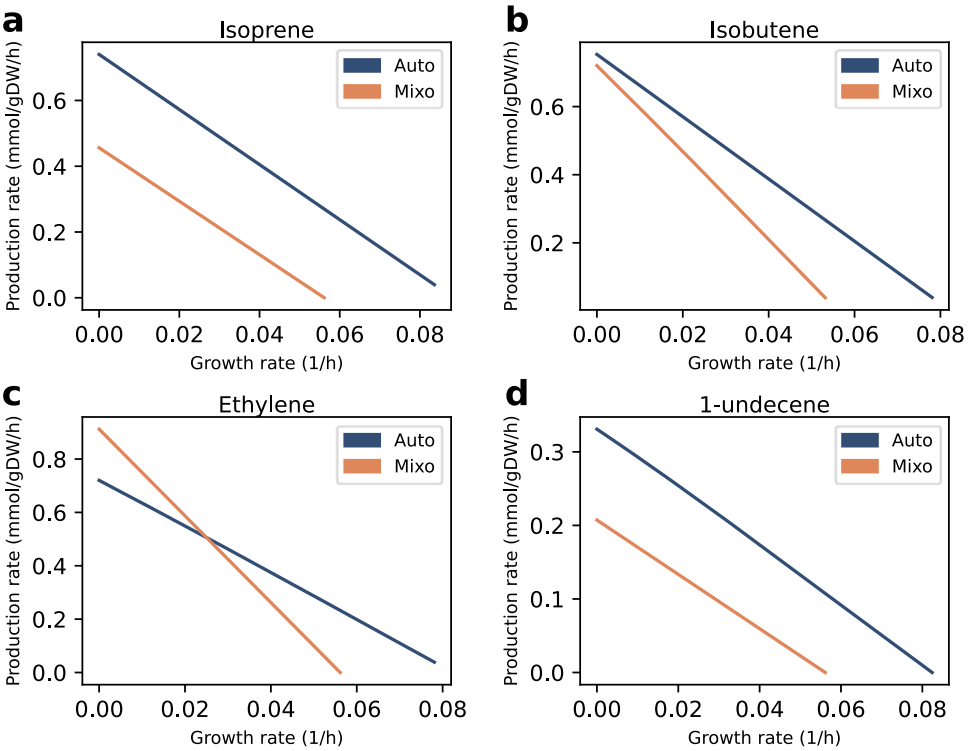

Fig. 2 Alkene-biomass phenotypic phase planes. a Isoprene. **b** Isobutene. **c** Ethylene. **d** 1-undecene. Phenotypic phase planes were obtained by varying these fluxes in the range from zero to maximal rate, under constant photon flux. Auto autotrophic, Mixo mixotrophic.

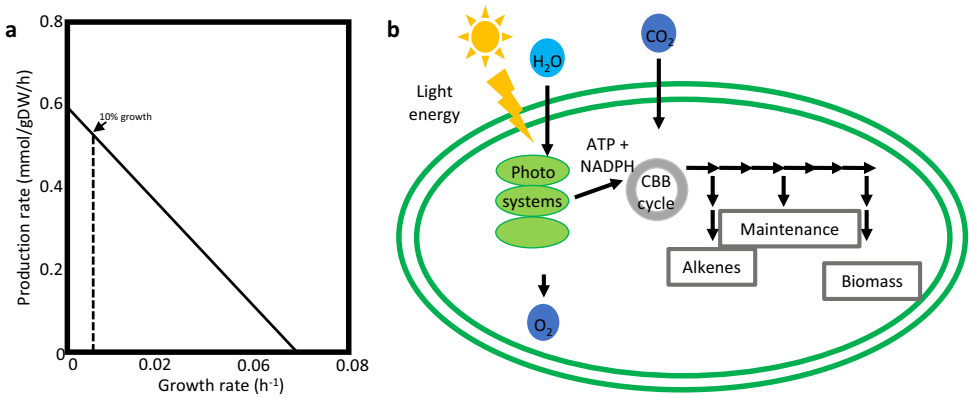

Fig. 3 Factors influencing the stoichiometric evaluation in this study. a As a trade-off occurs between biomass and alkene production, a two-step optimization strategy was performed, as described in the Methods section. **b** Cellular resources are allocated to biomass, cell maintenance and alkene production.

Table 2. Theoretical maximum productivity, mass yield and c-mol yield.

	Auto			Mixo		
Objective	Maximum productivity	Maximum theoretical mass yield	C-mol yield	Maximum productivity	Maximum theoretical mass yield	C-mol yield
Biomass	0.082			0.056		
Isoprene	0.67	0.20	0.90	0.41	0.41	0.90
Isobutene	0.68	0.20	0.87	0.51	0.42	0.90
Ethylene	0.65	0.15	0.65	0.82	0.34	0.73
1-undecene	0.30	0.21	0.91	0.19	0.42	0.90

Synechocystis was simulated to grow autotrophically and mixotrophically, when maximizing biomass and alkenes production. Maximum productivity is presented in units of h^{-1} or mmol/gDW/h, for biomass and alkenes, respectively. Mass yield is presented in units of gram product per gram substrate. Biomass yield is represented in units of gDW biomass per mmol carbon consumed. C-mol yield is presented in units of mol carbon produced per mol carbon consumed.
gDW gram dry-weight, *h* hour, *C* carbon, *Auto* autotrophic, *Mixo* mixotrophic.

Since the overall consumption and production rates are equal, under the steady-state assumption, the flux-sum serves as a proxy of the metabolite pool size in the system, by which the cellular ATP/NADPH ratio could be examined. The analysis revealed a narrow range of intracellular ATP pool (Table 1). In contrast, a larger variation in NADPH levels was determined. We computed that biomass accumulation required an ATP/NADPH ratio of 2.11 and 19.49, under autotrophic and mixotrophic conditions, respectively. In comparison, all the examined alkenes required ATP/NADPH ratios below the values for biomass (Table 1). Therefore, in order to attain a growth-coupled production, genetic interventions are needed to manipulate the cofactor pools[41]. A lower ATP availability could be achieved by introducing an "ATP-wasting" mechanism (e.g., ATPM)[42]. A higher cofactor availability of NAD(P)H could be achieved by the introduction of non-native NADH-dependent oxidoreductases, or protein engineering of enzymes for swapped cofactor-dependency[43].

It should be noted that, the ATP/NADPH ratios presented here slightly differ from earlier published results[44,45]. These differences could be justified by that: (i) Here, we considered flux in the entire metabolic network, whereas previous studies mainly considered photosynthetic reactions (e.g., ATPSu and NDH-1 and FNOR). (ii) Different metabolic network sized were examined, covering different number of reactions acting on ATP and NAD(P)H: 760 reactions[44], 780 reactions[45], and 883 reactions in this study. (iii) We simulated a synergistic interaction between biomass formation (10%) and alkene biosynthesis, whereas earlier studies modelled 0%[44] or 75%[45] of growth, which affected the evaluation of ATP/NAD(P)H demand.

Evaluation of intracellular flux distributions

In order to identify the metabolic reactions contributing to the computed turnover rates, we employed a reaction-centric approach by using pFBA. By comparing biomass and alkene-overproducing strains, potential reactions whose metabolic fluxes constrain alkenes synthesis in *Synechocystis* could be recognized. We would like to note that FBA and ^{13}C-metabolic flux analysis (MFA) are two different approaches to determine the intracellular fluxes[46]. Further, our model does not include information regarding cellular regulation or enzyme kinetics, which influence the conclusion on the flow of carbon in the cell.

Cofactor energy metabolism. Under both trophic growth modes, the majority of ATP generation was performed by the photosynthetic ATP synthetase (ATPSu) (Table 3). Under autotrophic conditions, a residual respiratory activity (ATPS4rpp_1) was determined for all objectives, but for the 1-undecene production. Our data are in line with earlier studies, showing that the respiratory pathway in *Synechocystis* is active also during light, albeit at low capacity[47]. Isoprene and ethylene production required a higher contribution of respiratory oxidative phosphorylation, whereas for isobutene, pyruvate kinase (PYK), from lower glycolysis, contributed to ATP generation (Table 3).

Reactions involved in ATP consumption were more diverse than for ATP generation and differed between growth conditions.

Table 3. Predicted flux distributions of cofactors-producing reactions.

		Biomass		Isoprene		Isobutene		Ethylene		1-undecene	
Trophy	Reaction	Flux	Percent	Flux	Percent	Flux	Percent	Flux	Percent	Flux	Percent
ATP											
Auto	ATPSu	16.04	98.28	16.19	96.85	15.84	91.98	15.04	98.09	14.46	99.95
	PYK	0.15	0.91	0.01	0.08	1.37	7.95	0.00	0.00	0.01	0.04
	ATPS4rpp_1	0.13	0.80	0.51	3.07	0.01	0.07	0.29	1.90	0.00	0.00
Mixo	ATPSu	10.70	99.99	10.50	100.00	11.10	95.25	13.44	98.65	10.76	99.96
	PYK	0.00	0.00	0.00	0.00	0.55	4.75	0.00	0.00	0.00	0.04
	ATPS4rpp_1	0.00	0.00	0.00	0.00	0.00	0.00	0.18	1.35	0.00	0.00
NADPH											
Auto	FNOR	7.56	97.66	10.15	99.82	10.92	99.83	7.50	88.09	10.94	99.77
	ICDHyr	0.10	1.33	0.01	0.10	0.01	0.09	0.98	11.56	0.01	0.09
	ME2	0.00	0.00	0.00	0.00	0.00	0.00	0.02	0.27	0.01	0.06
	MTHFD	0.06	0.78	0.01	0.06	0.01	0.06	0.01	0.07	0.01	0.05
Mixo	FNOR	0.02	3.02	1.76	94.84	3.20	86.62	3.73	69.72	2.37	99.28
	ICDHyr	0.07	12.76	0.01	0.38	0.01	0.19	1.24	23.14	0.01	0.29
	ME2	0.05	8.67	0.00	0.26	0.48	13.06	0.38	7.05	0.00	0.20
	MTHFD	0.04	7.49	0.00	0.22	0.00	0.09	0.00	0.08	0.00	0.17
	G6PDH2r	0.23	41.13	0.08	4.24	0.00	0.00	0.00	0.00	0.00	0.00
	GND	0.14	24.69	0.00	0.00	0.00	0.00	0.00	0.00	0.00	0.00
NADH											
Auto	GLYCLc	9E−03	4E + 00	9E−04	4E + 00	0E + 00	0E + 00	0E + 00	0E + 00	0E + 00	0E + 00
	HISTD	1E−02	6E + 00	1E−03	6E + 00	1E−03	2E−01	1E−03	1E−01	1E−03	8E + 00
	IMPD	1E−02	5E + 00	1E−03	5E + 00	1E−03	2E−01	1E−03	1E−01	1E−03	7E + 00
	IPMD	4E−02	2E + 01	4E−03	2E + 01	7E−01	1E + 02	4E−03	4E−01	4E−03	2E + 01
	MDH	7E−02	3E + 01	7E−03	3E + 01	7E−03	1E + 00	6E−01	7E + 01	0E + 00	0E + 00
	PGCD	1E−01	4E + 01	1E−02	4E + 01	1E−02	2E + 00	1E−02	1E + 00	1E−02	6E + 01
	P5CD	0E + 00	0E + 00	0E + 00	0E + 00	0E + 00	0E + 00	3E−01	3E + 01	0E + 00	0E + 00
Mixo	GLYCLc	6E−03	4E + 00	6E−04	5E + 00	0E + 00	0E + 00	6E−04	6E−02	0E + 00	0E + 00
	HISTD	1E−02	7E + 00	1E−03	8E + 00	1E−03	2E−01	1E−03	9E−02	1E−03	8E + 00
	IMPD	9E−03	7E + 00	9E−04	7E + 00	9E−04	2E−01	9E−04	8E−02	9E−04	7E + 00
	IPMD	3E−02	2E + 01	3E−03	2E + 01	5E−01	1E + 02	3E−03	3E−01	3E−03	2E + 01
	MDH	0E + 00	0E + 00	0E + 00	0E + 00	0E + 00	0E + 00	4E−01	4E + 01	0E + 00	0E + 00
	PGCD	8E−02	6E + 01	7E−03	5E + 01	6E−03	1E + 00	2E−01	2E + 01	8E−03	6E + 01
	P5CD	0E + 00	0E + 00	0E + 00	0E + 00	0E + 00	0E + 00	4E−01	4E + 01	0E + 00	0E + 00

Presented are percentage (%) and the corresponding flux (mmol/gDW/h) of reactions contributing to the generation of ATP and NAD(P)H. Zero flux indicates that the reaction carries no flux or <0.01 mmol/gDW/h. For the complete list of reactions, including their abbreviations, subsystem, lower and upper bounds, and stoichiometry, refer to data availability section.
Auto autotrophic, *Mixo* mixotrophic.

Under autotrophic growth, ATP consumption was dictated by reactions within CBB cycle and glycolysis/gluconeogenesis (phosphoglycerate kinase, PGK and phosphoribulokinase, PRUK) for all strains (Table 4). Earlier in vivo studies also determined PGK and PRUK as major ATP-consumers in *Synechocystis*[48,49]. Our data also revealed specific flux distributions depending on the objective function. For ethylene production, the ATP-consuming reactions were within nitrogen metabolism pathways (e.g., glutamine synthetase, GLNS), whereas for isoprene production, the terpenoid biosynthesis pathways contributed the most to ATP consumption. Bicarbonate transport (BCT1_syn) exhibited a large ATP consumption for production of isoprene and 1-undecene. Acetyl coenzyme A (acetyl-CoA) carboxylase (ACCOAC) was mainly involved in 1-undecene accumulation, probably due to high amount of carbon assimilated during the elongation process of fatty acyl chain for 1-undecene synthesis.

Reactions involved in ATP consumption were more diverse than for ATP generation and differed between growth conditions. Under autotrophic growth, ATP consumption was dictated by reactions within CBB cycle and glycolysis/gluconeogenesis (phosphoglycerate kinase, PGK and phosphoribulokinase, PRUK) for all strains (Table 4). Earlier in vivo studies also determined PGK and PRUK as major ATP-consumers in *Synechocystis*[48,49]. Our data also revealed specific flux distributions depending on the objective function. For ethylene production, the ATP-consuming reactions were within nitrogen metabolism pathways (e.g., glutamine synthetase, GLNS), whereas for isoprene production, the terpenoid biosynthesis pathways contributed the most to ATP consumption. Bicarbonate transport (BCT1_syn) exhibited a large ATP consumption for production of isoprene and 1-undecene. Acetyl coenzyme A (acetyl-CoA) carboxylase (ACCOAC) was mainly involved in 1-undecene accumulation, probably due to high amount of

Table 4. Predicted flux distributions of cofactors-consuming reactions.

		Biomass		Isoprene		Isobutene		Ethylene		1-undecene	
Trophy	Reaction	Flux	Percent	Flux	Percent	Flux	Percent	Flux	Percent	Flux	Percent
ATP											
Auto	PGK	−6.37	39.05	−8.02	47.97	−10.12	58.80	−4.89	35.87	−7.84	54.15
	PRUK	−3.50	21.43	−4.38	26.18	−5.77	33.52	−2.88	21.11	−3.95	27.29
	GLNS	−0.11	0.68	−0.01	0.07	−0.01	0.06	−1.09	8.00	−0.02	0.10
	ARGSS	−0.02	0.14	0.00	0.01	0.00	0.01	−0.41	3.02	0.00	0.02
	ACGK	−0.02	0.14	0.00	0.01	0.00	0.01	−0.41	3.02	0.00	0.02
	ACCOAC	−0.24	1.49	−0.02	0.15	−0.02	0.14	−0.02	0.12	−1.52	10.53
	BCT1_syn	0.00	0.00	−2.34	13.98	0.00	0.00	0.00	0.00	−0.54	3.72
	ADK1	−0.17	1.06	−0.02	0.10	−0.02	0.10	−1.01	7.38	−0.02	0.12
Mixo	PRUK	-0.17	1.56	−0.41	3.94	−2.06	17.63	−2.88	21.11	−0.19	1.76
	PGK	0.00	0.00	−0.45	4.31	−3.04	26.10	−4.89	35.87	−0.34	3.13
	GLNS	−0.52	4.85	−0.05	0.47	−0.05	0.43	−1.09	8.00	−0.05	0.48
	ARGSS	−0.02	0.14	0.00	0.01	0.00	0.01	−0.41	3.02	0.00	0.01
	ACGK	−0.02	0.14	0.00	0.01	0.00	0.01	−0.41	3.02	0.00	0.01
	ACCOAC	−0.17	1.55	−0.02	0.16	−0.02	0.14	−0.02	0.12	−0.95	8.82
	ADK1	−0.12	1.10	−0.01	0.11	−0.01	0.10	−1.01	7.38	−0.01	0.11
	CYPHYS	−6.08	56.83	0.00	0.00	−5.27	45.18	0.00	0.00	−8.53	79.18
	ATPM	0.00	0.00	−7.96	75.80	0.00	0.00	0.00	0.00	0.00	0.00
NADPH											
Auto	GAPDi_nadp	−6.37	82.30	−8.02	78.86	−10.12	92.53	−7.78	91.35	−7.84	71.43
	KARA1	−0.07	0.89	−0.01	0.07	−0.68	6.26	−0.01	0.08	−0.01	0.06
	3OAR60	−0.03	0.44	0.00	0.03	0.00	0.03	0.00	0.04	−0.30	2.77
	DXPRIi	−0.01	0.19	−0.67	6.61	0.00	0.01	0.00	0.02	0.00	0.01
Mixo	GAPDi_nadp	0.00	0.00	−0.45	24.46	−3.04	82.44	−4.89	91.33	−0.34	14.13
	KARA1	−0.05	8.55	0.00	0.25	−0.52	14.03	0.00	0.09	0.00	0.20
	3OAR60	−0.02	4.25	0.00	0.13	0.00	0.06	0.00	0.04	−0.19	7.92
	DXPRIi	−0.01	1.83	−0.41	22.22	0.00	0.03	0.00	0.02	0.00	0.04
NADH											
Auto	NDH1_2u	−0.11	44.84	−0.01	44.84	−0.69	97.87	−0.59	60.30	0.00	0.00
	HSDxi	−0.05	21.52	−0.01	21.52	−0.01	0.75	−0.01	0.54	−0.01	30.12
	ALAD_L	−0.04	15.73	0.00	15.73	0.00	0.00	0.00	0.21	0.00	11.73
	P5CRx	−0.02	7.95	0.00	7.95	0.00	0.28	0.00	0.20	0.00	11.13
	GLUSx	0.00	0.00	0.00	0.00	0.00	0.00	−0.37	38.31	0.00	22.77
	MTHFR2	−0.01	4.13	0.00	4.13	0.00	0.14	0.00	0.10	0.00	5.78
Mixo	HSDxi	−0.04	26.42	0.00	29.81	0.00	0.68	0.00	0.33	0.00	28.43
	ALAD_L	−0.03	19.28	0.00	21.76	0.00	0.38	0.00	0.15	0.00	0.00
	P5CRx	−0.01	9.76	0.00	11.01	0.00	0.25	0.00	0.12	0.00	10.50
	GLUSx	−0.04	32.29	0.00	23.56	−0.04	7.34	−1.08	99.07	0.00	31.96
	MTHFR2	−0.01	5.07	0.00	5.72	0.00	0.13	0.00	0.06	0.00	5.46

Presented are percentage (%) and the corresponding flux (mmol/gDW/h) of reactions contributing to the consumption of ATP and NAD(P)H. Zero flux indicates that the reaction carries no flux or <0.01 mmol/gDW/h. For the complete list of reactions, including their abbreviations, subsystem, lower and upper bounds, and stoichiometry, refer to data availability section.
Auto autotrophic, *Mixo* mixotrophic.

carbon assimilated during the elongation process of fatty-acyl chain for 1-undecene synthesis.

Under mixotrophic conditions, the ATP consumption was mainly governed by cyanophycin metabolism (cyanophycin synthetase, CYPHYS) during biomass, isobutene and 1-undecene synthesis (Table 4). For isoprene accumulation, ATP maintenance (ATPM) accounted for the majority of ATP consumption (Table 4). As ATPM contributes to cellular functions other than growth (e.g., turgor pressure) (Fig. 3b), it can be inferred that a hyper-producing isoprene strain would more likely become ATP-limited when grown mixotrophically, as compared to the other alkene-producing strains.

We additionally investigated how the ATP precursors (ADP, AMP and Pi) are recycled within the metabolic network (Fig. 6, Supplementary Tables 9–12 and Supplementary Figs. 11–19). The stoichiometric analysis revealed that, under both autotrophic and mixotrophic growth, the de novo adenosine biosynthesis, downstream to phosphoribosylpyrophosphate synthetase (PRPPS), contributed equally to all objectives but ethylene production (Fig. 6, Supplementary Table 9 and Supplementary

Figs. 11–19). The salvage adenosine pathway through adenylate kinase (ADK1) contributes the most to ADP-AMP cycling during ethylene (Supplementary Tables 7 and 10 and Supplementary Figs. 16–17) and biomass overproduction (Fig. 6 and Supplementary Table 7). For ethylene synthesis, argininosuccinate synthase (ARGSS) in arginine metabolism showed enhanced flux to produce AMP (Fig. 5a, Supplementary Fig. 10 and Supplementary Table 9). Of note, phosphoketolase (PKETF) was shown to be a common consumer of Pi for the production of all objective functions (Fig. 4, and Supplementary Table 12).

The enhanced ADK1 flux during biomass (Fig. 6, Supplementary Fig. 11 and Supplementary Tables 7 and 10) and ethylene production (Supplementary Figs. 16–17 and Supplementary Tables 7 and 10) presumably sustains the increase in respiration rate, by providing more ADP to the oxidative phosphorylation pathway. A prior study revealed that low respiration rate is a possible limiting factor of ethylene production through ethylene-forming enzyme (EFE) in *Saccharomyces cerevisiae*[50], and could explain the low ethylene production found experimentally in *Synechocystis*[36].

Based on our studies and others[51], we suggest that a combinatorial metabolic engineering, with the aim to form an efficient ATP cycling for fueling the CBB cycle, could be based on the ATP-consuming enzymes (e.g., PRUK and PGK), and on the ATP-producing enzymes (i.e., PYK). In addition a high ATP turnover would be beneficial for the heterologous production of alkenes, and probably other products, in *Synechocystis*, as previously confirmed for *E. coli*[42].

We propose that, under mixotrophic conditions, the regeneration of cellular nitrogenous polymers (e.g., cyanophycin) is essential for optimized nitrogen and energy metabolism in the cell. The data are in agreement with previous studies, arguing that the transition in growth conditions affects nitrogen metabolism through cyanophycin[52].

Cofactor redox metabolism. In agreement with earlier reports[10,53], the flux analysis revealed that, under both autotrophic and mixotrophic growth, the photosynthetic ferredoxin-$NADP^+$ reductase (FNOR) contributed largely to the supply of NADPH (Table 3). An exception was noted for biomass production, under mixotrophic conditions, for which NADPH was produced by the oxidative pentose phosphate pathway (Table 3). In relation to the calculated ATP/NADPH ratios (Table 1), we presume that the high ratio determined for biomass production under mixotrophic conditions stems from the lower flux through the FNOR, as compared to that as seen for the other objectives.

In the ethylene-overproducing strain, the flux through isocitrate dehydrogenase (ICDHyr) was significantly higher than that in the other modeled strains (Table 3 and Supplementary Figs. 6–7). We suggest that ICDHyr is a good candidate for enhanced production of TCA-derived molecules, such as ethylene, supported by the results from studies on engineered ethylene-producing strain of *Synechocystis*[54].

The flux distribution of reactions catalyzing NADPH consumption revealed that for all objectives, NADPH was mainly consumed by glyceraldehyde-3-phosphate dehydrogenase (GAPDi_nadp), a key enzyme within the CBB cycle and gluconeogenesis (Table 4). As could be expected, the flux though ketol-acid reductoisomerase (KARA1) within the branched-chain amino acids (BCAA) biosynthesis was enhanced for isobutene production, and reaction fluxes though the terpenoid and fatty acids pathways (i.e., fatty-acyl reductases) were increased for isoprene and 1-undecene.

Though carrying low flux under both growth conditions, production of NADH were distributed among BCAA biosynthesis pathway (3-isopropylmalate dehydrogenase, IPMD), TCA cycle (malate dehydrogenase, MDH) and L-arginine and L-proline metabolism (phosphoglycerate dehydrogenase, PGCD) (Table 3). Notably, an enzyme from the L-arginine and L-proline metabolism (Δ1-pyrroline-5-carboxylate dehydrogenase, P5CD) was found to be predominant during ethylene overproduction (Fig. 5b).

We observed that under autotrophy, for all objectives but 1-undecene, the photosynthesis (NAD(P)H dehydrogenase, NDH1_2u) is the main NADH consumer (Table 4). For 1-undecene, L-lysine metabolism (L-homoserine dehydrogenase, HSDxi) contributed the most. HSDxi and L-alanine metabolism (L-alanine dehydrogenase, ALAD_L) were major NADH consumers for biomass, isoprene, isobutene and 1-undecene production. For ethylene production, nitrogen metabolism was a key NADH consumer (e.g., L-glutamate synthase, GLUSx).

The data imply that the regeneration of the NADH pool in the system is facilitated mainly by amino acids metabolism. The reduction of nitrate to ammonia requires a considerable amount of NADPH. We suggest that designing an alternative NADH-dependent pathway for ammonium assimilation (for example by introducing ALAD_L) could reduce the competition for NADPH. Hence, increasing the potential for NADPH-dependent product formation (Fig. 1), while simultaneously enabling nitrogen cycling in the cell.

We additionally investigated the redox balancing mechanism by the (de)phosphorylating enzymes, and identified that NAD kinase (NADK) had a negligible contribution to the overall flux of NAD^+ consumption (Supplementary Table 7). As $NADP^+$ serves as the final electron acceptor of photosystem I[10], this finding was rather surprising. The role of NADK only begins to be elucidated[55,56], and the functionality of $NADP^+$ phosphatase remains to be discovered.

Considering the large variation in NADPH turnover rates (Table 1), we postulate that, under light-limited conditions, the ATP/NADPH ratios are mainly governed by the reduction of $NADP^+$, rather than by the regeneration of ATP. Our data are consistent with a previous study, demonstrating that, under steady-state photosynthesis, CO_2 assimilation is not limited by the availability of ATP, but by the rate of NADPH formation[57].

Energy and redox balance are interlinked with the production of central metabolites. Our findings show that balancing the intracellular ratio of ATP and NADPH is directly interconnected with and influence the regeneration of central carbon metabolites (i.e., pyruvate and acetyl-CoA). We identified that, under autotrophic conditions, carbon is channeled back to the Embden-Meyerhof-Parnas (EMP) pathway to synthetize glycogen through glucose-1-phosphate adenylyltransferase (GLGC) and glycogen synthase (GLCS1) reactions (Fig. 4 and Supplementary Figs. 2, 4, 6). In *Synechocystis*, glycogen metabolism was shown to act as an ATP-buffering system, and the inactivation of GLGC led to an increased NADPH pool[58,59]. It has furthermore been reported that glycolytic routes form anaplerotic shunts that replenish metabolites for carbon fixation by the CBB cycle[60]. We suggest that gluconeogenesis and glycogen turnover should be considered within future bioengineering research. This is in contrast to a number metabolic engineering studies, in which a glycogen-deficient *Synechocystis* strain is used as chassis for production[61,62].

Pyruvate kinase (PYK) and Malic enzyme (ME2) are the major contributors to pyruvate synthesis, although at distinct ratios, depending on the objective function (Supplementary Table 13). The data are in accordance with previous reports, suggesting that due to allosteric-inhibition of PYK by its product, ATP[63], ME2 functions as an additional route for synthesizing pyruvate in *Synechocystis*[7]. Fluxomic studies pinpointed that PYK reaction represents a bottleneck for isobutyraldehyde production in *Synechococcus elongatus* PCC 7942, which was overcome by heterologous overproduction of PYK[64]. Under mixotrophic conditions, the Entner–Doudoroff pathway also provided pyruvate for biomass synthesis (Supplementary Table 13). Hence, based on pure stoichiometry, and in agreement with previous research, we suggest that PYK and ME2 are good candidates for metabolic engineering of

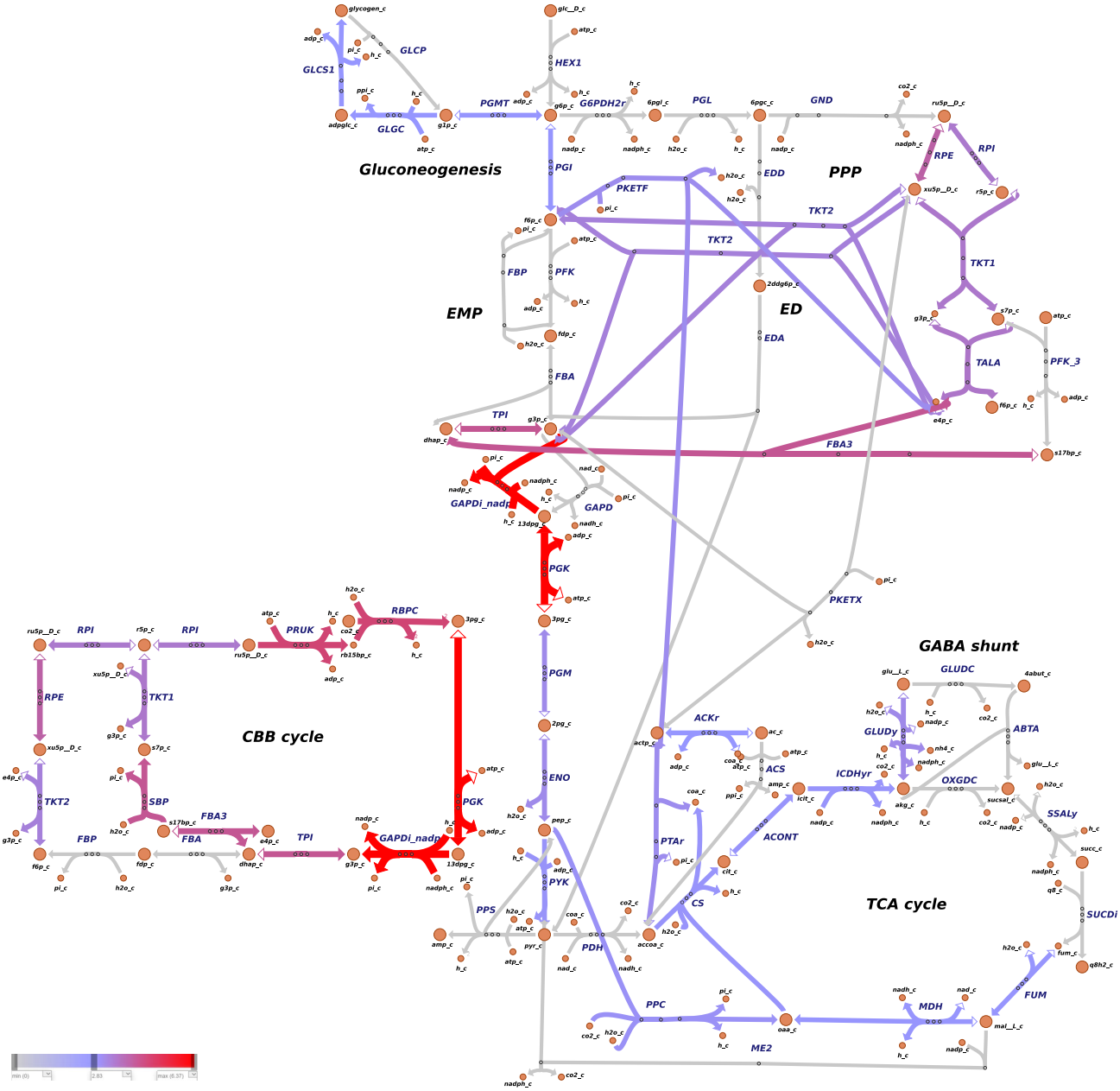

Fig. 4 Metabolic flux map of central carbon metabolism for *Synechocystis* sp. PCC 6803. *Synechocystis* was simulated to grow under autotrophic conditions, with biomass set as objective. Reaction rates (mmol/gDW/h) were predicted using pFBA[69]. Note that, the colors associated with the fluxes are relative to the other reactions rates presented in the map. Irreversible reactions are indicated by one-headed arrows; reversible reactions are indicated by two-headed arrows. For reaction directionality, refer to the data availability section. For metabolic flux maps of central carbon metabolism for biomass simulated to grow mixotrophic conditions, and other objectives simulated to grow under auto- and mixotrophic conditions, refer to Supplementary Figs. 1–9. The map was generated with Escher web-tool[72]. Metabolic reactions and metabolites are indicated by their BiGG identifier[73]. TCA tricarboxylic acid, GABA branched-chain amino acids γ-aminobutyrate, CBB Calvin–Benson–Bassham, ED Entner–Doudoroff, EMP Embden-Meyerhof-Parnas, PPP pentose phosphate pathway.

Synechocystis for hydrocarbon production. The CO_2 released by ME2 can be further assimilated by phosphoenolpyruvate carboxylase (PPC) (Fig. 4), thus resulting in a net zero carbon loss and a high product yield.

Interestingly, and less intuitively, IPMD within the isobutene biosynthesis pathway (Fig. 1), showed a high contribution for redox recycling in biomass, isoprene and 1-undecene biosynthesis as well (Table 3). In cancer research, it was shown that the TCA cycle in tumor cells is heavily fed by acetyl-CoA derived from BCAA[65]. Taken together, we presume that, the catabolism of BCAA provides an alternative route for the synthesis of acetyl-CoA - a key precursor molecule for many cellular biosynthesis pathways, including terpenoids and lipids.

Our results further emphasize the essentiality of metabolic shortcuts in central carbon metabolism for attaining effective metabolic states[66]. We show that acetate metabolism through phosphoketolase serves as an efficient carbon- and energy-recycling pathway for cell maintenance, as suggested in a biochemical study focusing on the role of phosphoketolase in cyanobacteria[67].

Serine and glycine metabolism represents an uncharacterized pathway for cellular energy and redox homeostasis in Synechocystis.

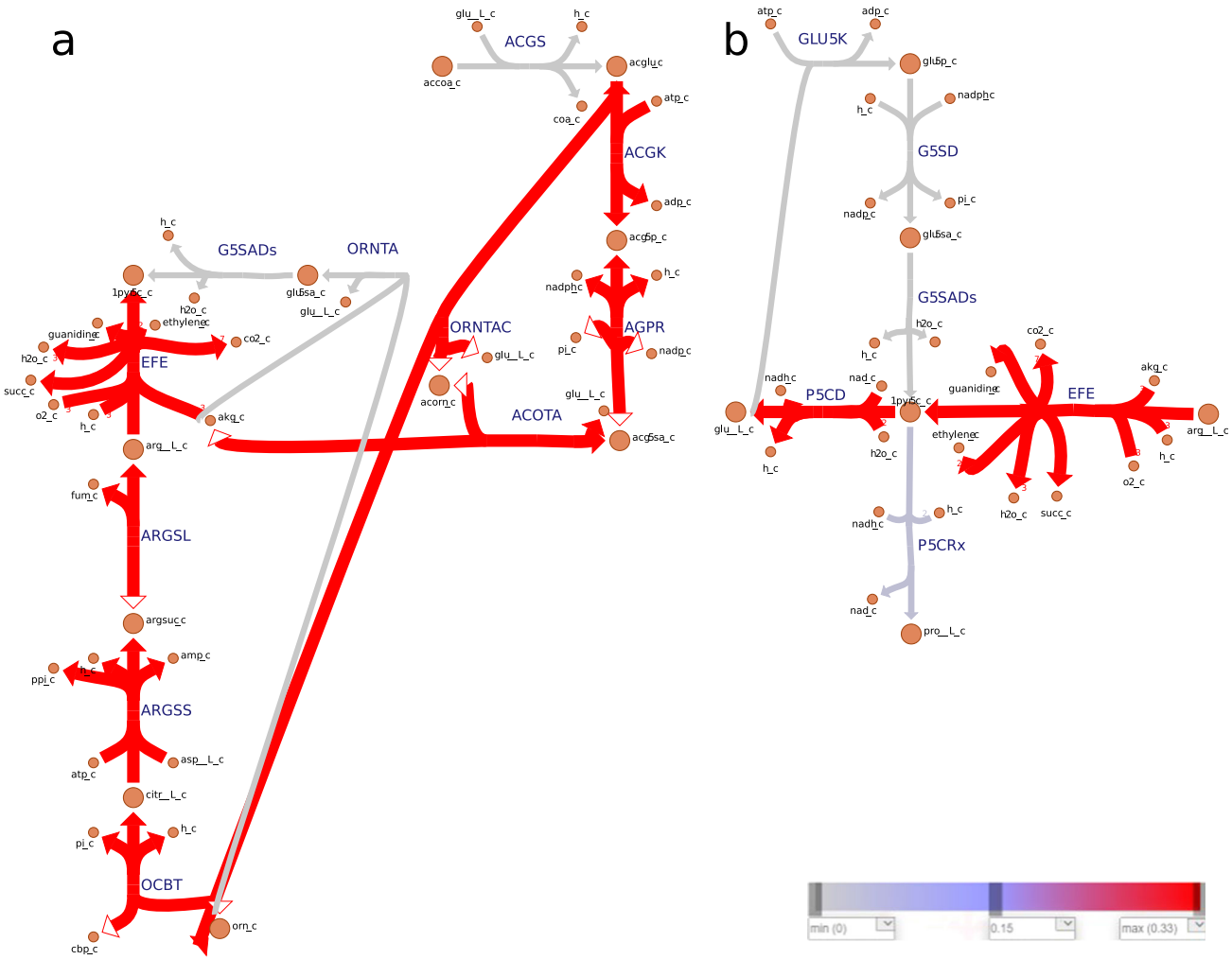

Fig. 5 Metabolic flux map of nitrogen metabolism for *Synechocystis* sp. PCC 6803. *Synechocystis* was simulated to grow under autotrophic conditions, with ethylene set as objective. Reaction rates (mmol/gDW/h) were predicted using pFBA[69]. **a** L-glutamate and L-arginine regeneration through the urea cycle. **b** L-glutamate and L-proline regeneration. Note that, the colors associated with the fluxes are relative to the other reactions rates presented in the map. Irreversible reactions are indicated by one-headed arrows; reversible reactions are indicated by two-headed arrows. For reaction directionality see data availability section of the GitHub repository. For metabolic flux maps of nitrogen metabolism for *Synechocystis* sp. PCC 6803 with ethylene set as objective, simulated to grow under mixotrophic conditions, refer to Supplementary Fig. 10. The map was generated with Escher web-tool[72]. Metabolic reactions and metabolites are indicated by their BiGG identifier[73].

We show that FBA is a powerful tool to investigate cellular metabolism globally and highlight flux patterns, by which new routes could be found and serve as basis for future studies. We learned that reactions participating in the L-serine synthesis, one-carbon metabolism and the glycine cleavage system (SOG pathway) function as an auxiliary pathway to regenerate ATP, NADPH and NADH in *Synechocystis*. Fluxes through SOG were identified when maximizing biomass and alkenes production (Fig. 6, Supplementary Tables 9–12 and Supplementary Figs. 11–19). The discovery that SOG pathway contributes to the biosynthetic requirements of ATP and NADPH of high-proliferating cells[68], strengthens our suggestion that SOG deserves a thorough investigation for metabolic engineering of *Synechocystis*.

To conclude, we demonstrate the significance of high flexibility in activity of energy- and carbon-converting enzymes in order to achieve the required ATP/NADPH output ratio. It was apparent that the overall activity of the *Synechocystis* metabolism is governed by several high-flux core reactions, which probably allows the cell to adapt rapidly to perturbations in environmental conditions and genetic modifications. We also show that assessment of ATP and NAD(P)H balance can neither be done in isolation from each other and their precursors, nor from carbon and nitrogen metabolism. Even though the predictions are yet to be validated in vivo, our results provide hints for strain design strategies enabling efficient bioproduction of valuable compounds derived from core metabolic pathways in *Synechocystis*.

METHODS

Computational tools

Parsimonious enzyme usage FBA (pFBA)[69] was employed on COBRApy v0.20.0[70] using the commercial solver Gurobi v10.0.1 (Gurobi Optimization, Inc., Houston, TX, United States) in Python v3.8.5, using the packages Pandas v1.3.0, NumPy v1.19.4, Matplotlib v3.3.3 and Pickle v4.0. Model consistency was tested with MEMOTE v0.12.0[71]. Visualization of the metabolic reaction network and the obtained fluxes was done using the Escher web-tool[72].

Metabolic network reconstruction

The iJN678 genome-scale metabolic model of *Synechocystis* sp. PCC 6803[19], downloaded from the BiGG database[73], was used for

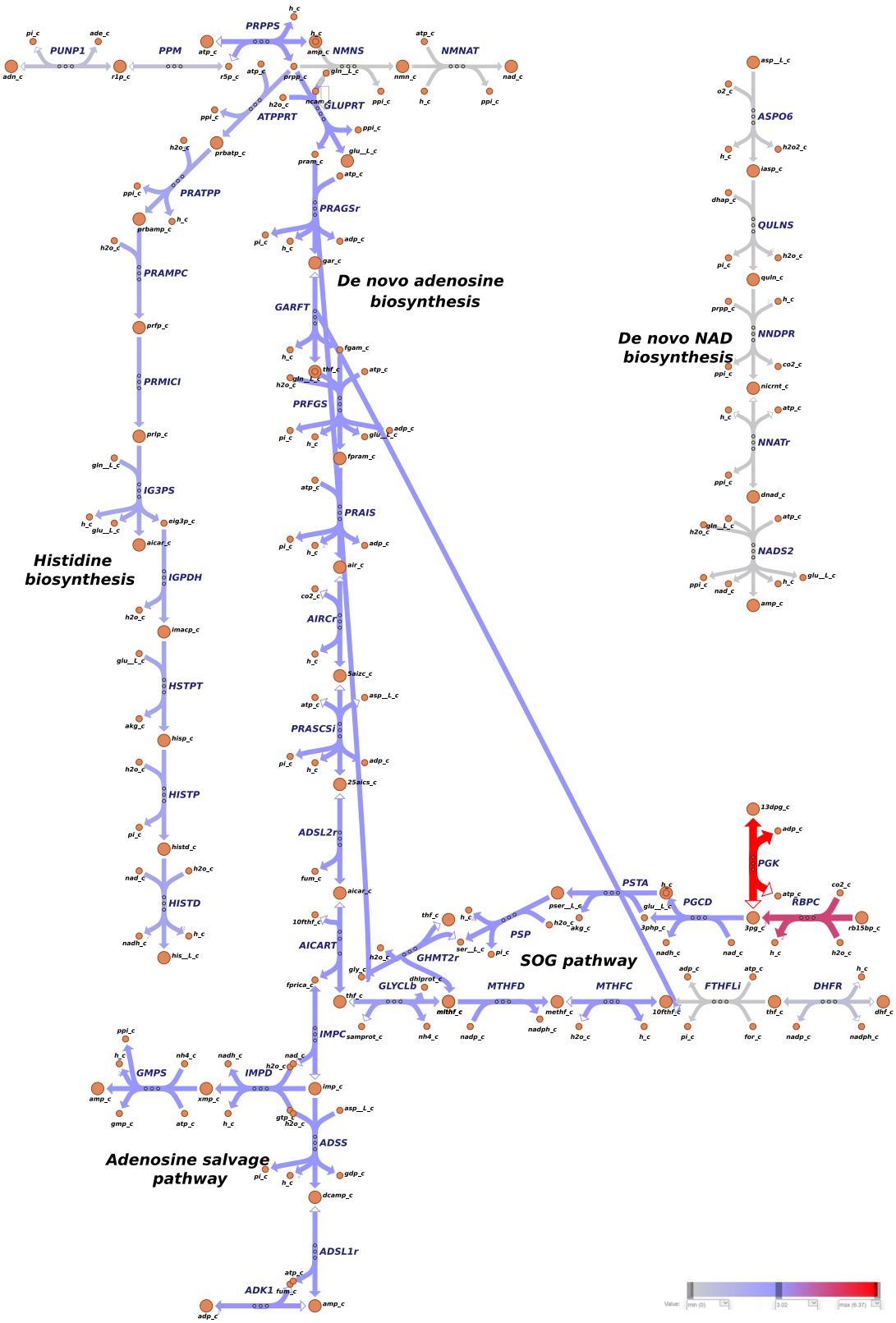

Fig. 6 Metabolic flux map of ATP and NAD de novo and salvage metabolism for *Synechocystis* sp. PCC 6803. *Synechocystis* was simulated to grow under autotrophic conditions, with biomass set as objective. Reaction rate (mmol/gDW/h) were predicted using pFBA[69]. Note that, the colors associated with the fluxes are relative to the other reactions rates presented in the map. Irreversible reactions are indicated by one-headed arrows; reversible reactions are indicated by two-headed arrows. For reaction directionality, refer to the data availability section. For metabolic flux maps of central carbon metabolism for biomass simulated to grow mixotrophic conditions, and other objectives simulated to grow under auto- and mixotrophic conditions, refer to Supplementary Figs. 11–19. The map was generated with Escher web-tool[72]. Metabolic reactions and metabolites are indicated by their BiGG identifier[73]. NAD nicotinamide adenine dinucleotide, SOG serine, one-carbon cycle, glycine synthesis.

the computational analysis. The model reconstruction includes 622 genes, 863 reactions and 795 metabolites. iJN678 also contains three different biomass compositions, allowing for simulating autotrophic, mixotrophic, and heterotrophic growth conditions, in addition to constraining the appropriate carbon and photon uptake rates.

The metabolic network was updated in accordance with the literature, yielding iJN678_AK, (Supplementary Table 1), as follows: addition of the tricarboxylic acid (TCA) cycle shunt reactions[74–76], addition of the phosphoketolase reactions[67,77], addition of the Entner–Doudoroff (ED) pathway[78], addition of the light-independent L-serine biosynthesis pathway[79], addition of prephenate transaminase, prephenate dehydratase and arogenate dehydrogenase[80], transhydrogenase (NADTRHD) was changed to a reversible reaction[11], addition of NADH dehydrogenase 2, alternative respiratory terminal oxidase, and flavodiiron proteins 2 and 4, and constraining cytochrome b6f, cytochrome c oxidase and NAD(P)H dehydrogenase to zero[47,81]. In addition, non-growth associated ATP maintenance (ATPM)[82,83] reaction was added to the model. The ATPM coefficient is represented by a pseudo-reaction that degrades ATP into ADP and orthophosphate (Pi) (Eq. 1).

$$ATP + H_2O \rightarrow ADP + Pi + H \quad (1)$$

For the evaluation of heterologous alkene production in *Synechocystis*, four biosynthesis pathways[34–36,84] were separately implemented into the iJN678_AK model, yielding iJN678_AK_isoprene, iJN678_AK_isobutene, iJN678_AK_ethylene and iJN678_AK_1-undecene (Supplementary Tables 2–5). In each reconstructed model, a cytoplasmatic export reaction for each alkene was introduced and set as the objective function. The resulting metabolic network reconstructions are encoded in SBML format (Systems Biology Markup Language)[85], and are available in the GitHub repository https://github.com/amitkugler/CBA.

Constraint-based modeling

To evaluate the steady-state flux distributions, we employed pFBA[69], in which the objective function is optimized using FBA, followed by the minimization of total absolute flux through all gene-associated reactions (Eqs. 2–5).

$$maximize\, Z = c^T \cdot v \quad (2)$$

s.t

$$\sum_{j=1}^{n} S_{ij} \cdot v_j = 0 \quad (3)$$

$$v_j^{LB} \le v_j \le v_j^{UB} \quad (4)$$

s.t

$$minimize \sum_{j=1}^{m} \left| v_{irrev,j} \right| \quad (5)$$

Where Z is the objective function, v is the flux vector of the metabolic reactions, c^T is the transposed vector of the objective coefficient. S_{ij} refers to the stoichiometric coefficient of metabolite i participating in reaction j, and the v_j refers to the vector of reaction flux (mmol/gDW/h; gDW, gram dry weight) of reaction j at steady state. The flux v_j is the j-th component of an n-dimensional flux vector v, where n is the total number of fluxes, m is the number of gene-associated irreversible reactions (v_{irrev}). LB and UB correspond to the lower bound and upper bound, respectively, of the j-th reaction in the flux vector v. Equation 3 can also be used to distinguish between reversible and irreversible reactions, where $v_j^{LB} = 0$ for the latter.

To explore the flux solution space, flux variability analysis (FVA)[86] was performed. The fraction of the optimum was set to 95%, which accounts for 5% variation around the best-known objective value. The FVA revealed infinite bounds for transhydrogenase (NADTRHD), irreversible leucine transaminase (LEUTAi) and glycine cleavage system (GLYCL and GLYCL_2). It was reported earlier that, the transhydrogenase reaction was poorly resolved by ^{13}C measurements[87]. Therefore, we chose to model redox balance without an active NADTRHD, as previously suggested[88]. At the same time, we could learn how the entire metabolic network balances between NADPH/NADH. In addition, the upper and lower bounds of LEUTAi and GLYCL and GLYCL_2 were constrained to zero, and the glycine cleavage system was modeled by introducing three separate reactions (Supplementary Table 1).

In order to avoid thermodynamic infeasible cycles, the "add_loopless" function in COBRApy was applied, that makes thermodynamically infeasible loops impossible[89]. In addition, we coupled our analysis to FVA.

According to previous studies[7,90], autotrophic metabolism was simulated by constraining the carbon dioxide, bicarbonate and glucose uptake rates to 0, 3.7 and 0 mmol/gDW/h, respectively. Mixotrophic metabolism was simulated by constraining the inorganic carbon (carbon dioxide and bicarbonate) uptake rates to 0 and glucose uptake rate to 0.38, respectively. For both trophic conditions, the photon uptake rate to was set to 45 mmol/gDW/h, to simulate a light-limited condition. These settings resulted in maximum specific growth rates of 0.082 h^{-1} and 0.056 h^{-1}, under autotrophic and mixotrophic conditions, respectively, which are in agreement with experimental growth values[7,22]. In addition, the biomass objective function[91] was set to BIOMASS_Ec_SynAuto, BIOMASS_Ec_SynMixo, depending on the simulated growth conditions, to account for changes in macromolecular composition.

Two-step optimization strategy

Following earlier studies[92,93], showing that a feasible overproduction of hydrocarbons in *Synechocystis* entails a carbon partitioning to biomass of 10%, we simulated a scenario where the cellular growth is limited, while achieving a high alkene production rate. We used a two-step optimization strategy, where, first, the biomass objective function was maximized. Then, the minimum flux through the biomass objective function was set to 10% of the obtained value, followed by the maximization of alkene production.

Evaluation of production strains

For providing a global perspective on the relation between growth rate and alkene production a phenotypic phase plane analysis[38] was carried out.

The flux-sum analysis was used to quantify the cofactors turnover rates among the metabolic network[39]. The flux-sum values for a metabolite represent the sum of flux in all the reactions that consume or produce it, multiplied by the corresponding stoichiometric coefficients (Eq. 6).

$$\Phi_i = \sum_{j \epsilon P_i} S_{ij} \bullet v_j = \sum_{j \epsilon C_i} S_{ij} \bullet v_j = 0.5 \sum_j |S_{ij} \bullet v_j| \quad (6)$$

Where P_i denotes the set of reactions producing metabolite i, and C_i denotes the set of reactions consuming metabolite i. Under the steady-state conditions, the consumption and production rates for any metabolite are equal. Thus, the turnover rate of metabolite i is half the absolute sum of consumption and the generation rates.

The theoretical maximum productivity is expressed h^{-1} or mmol/gDW/h for biomass and alkenes, respectively. The theoretical maximum yield is expressed as gram product produced per gram of substrate consumed. The carbon-conversion efficiency was estimated by calculating carbon-mole (c-mole) produced per c-mole of substrate consumed.

Reporting summary

Further information on research design is available in the Nature Research Reporting Summary linked to this article.

DATA AVAILABILITY

All the data supporting the work are available within the paper, its supplementary material, and in the GitHub repository https://github.com/amitkugler/CBA.

CODE AVAILABILITY

The models and the code used for this study can be found in the GitHub repository https://github.com/amitkugler/CBA.

Received: 23 October 2022; Accepted: 1 September 2023;
Published online: 22 September 2023

REFERENCES

1. Satta, A., Esquirol, L. & Ebert, B. E. Current metabolic engineering strategies for photosynthetic bioproduction in cyanobacteria. *Microorganisms* **11**, 455 (2023).
2. Liu, X., Miao, R., Lindberg, P. & Lindblad, P. Modular engineering for efficient photosynthetic biosynthesis of 1-butanol from CO_2 in cyanobacteria. *Energy Environ. Sci.* **12**, 2765–2777 (2019).
3. Rodrigues, J. S. & Lindberg, P. Metabolic engineering of *Synechocystis* sp. PCC 6803 for improved bisabolene production. *Metab. Eng. Commun.* **12**, e00159 (2021).
4. Kukil, K. & Lindberg, P. Expression of phenylalanine ammonia lyases in *Synechocystis* sp. PCC 6803 and subsequent improvements of sustainable production of phenylpropanoids. *Microb. Cell Fact.* **21**, 8 (2022).
5. Matson, M. M. & Atsumi, S. Photomixotrophic chemical production in cyanobacteria. *Curr. Opin. Biotechnol.* **50**, 65–71 (2018).
6. Liu, N., Santala, S. & Stephanopoulos, G. Mixed carbon substrates: a necessary nuisance or a missed opportunity? *Curr. Opin. Biotechnol.* **62**, 15–21 (2020).
7. Yang, C., Hua, Q. & Shimizu, K. Metabolic flux analysis in *Synechocystis* using isotope distribution from ^{13}C-labeled glucose. *Metab. Eng.* **4**, 202–216 (2002).
8. Lee, T.-C. et al. Engineered xylose utilization enhances bio-products productivity in the cyanobacterium *Synechocystis* sp. PCC 6803. *Metab. Eng.* **30**, 179–189 (2015).
9. Kanno, M., Carroll, A. L. & Atsumi, S. Global metabolic rewiring for improved CO_2 fixation and chemical production in cyanobacteria. *Nat. Commun.* **8**, 14724 (2017).
10. Cruz, J. A. Plasticity in light reactions of photosynthesis for energy production and photoprotection. *J. Exp. Bot.* **56**, 395–406 (2004).
11. Kämäräinen, J. et al. Pyridine nucleotide transhydrogenase PntAB is essential for optimal growth and photosynthetic integrity under low-light mixotrophic conditions in *Synechocystis* sp. PCC 6803. *N. Phytol.* **214**, 194–204 (2017).
12. Kramer, D. M. & Evans, J. R. The importance of energy balance in improving photosynthetic productivity. *Plant Physiol.* **155**, 70–78 (2011).
13. Joliot, P. & Joliot, A. Cyclic electron transfer in plant leaf. *Proc. Natl Acad. Sci.* **99**, 10209–10214 (2002).
14. Makino, A., Miyake, C. & Yokota, A. Physiological functions of the water–water cycle (Mehler reaction) and the cyclic electron flow around PSI in rice leaves. *Plant Cell Physiol.* **43**, 1017–1026 (2002).
15. Gao, H. & Xu, X. The cyanobacterial NAD kinase gene sll1415 is required for photoheterotrophic growth and cellular redox homeostasis in *Synechocystis* sp. strain PCC 6803. *J. Bacteriol.* **194**, 218–224 (2012).
16. Chen, X., Li, S. & Liu, L. Engineering redox balance through cofactor systems. *Trends Biotechnol.* **32**, 337–343 (2014).
17. Yang, H., Jia, X. & Han, Y. Microbial redox coenzyme engineering and applications in biosynthesis. *Trends Microbiol.* **30**, 318–321 (2022).
18. Park, J. & Choi, Y. Cofactor engineering in cyanobacteria to overcome imbalance between NADPH and NADH: A mini review. *Front. Chem. Sci. Eng.* **11**, 66–71 (2017).
19. Nogales, J., Gudmundsson, S., Knight, E. M., Palsson, B. O. & Thiele, I. Detailing the optimality of photosynthesis in cyanobacteria through systems biology analysis. *Proc. Natl Acad. Sci.* **109**, 2678–2683 (2012).
20. Fu, P. Genome-scale modeling of *Synechocystis* sp. PCC 6803 and prediction of pathway insertion. *J. Chem. Technol. Biotechnol.* **84**, 473–483 (2009).
21. Montagud, A., Navarro, E., Fernández de Córdoba, P., Urchueguía, J. F. & Patil, K. R. Reconstruction and analysis of genome-scale metabolic model of a photosynthetic bacterium. *BMC Syst. Biol.* **4**, 156 (2010).
22. Shastri, A. A. & Morgan, J. A. Flux balance analysis of photoautotrophic metabolism. *Biotechnol. Prog.* **21**, 1617–1626 (2005).
23. Knoop, H. et al. Flux balance analysis of cyanobacterial metabolism: the metabolic network of *Synechocystis* sp. PCC 6803. *PLoS Comput. Biol.* **9**, e1003081 (2013).
24. Yoshikawa, K. et al. Reconstruction and verification of a genome-scale metabolic model for *Synechocystis* sp. PCC 6803. *Appl. Microbiol. Biotechnol.* **92**, 347–358 (2011).
25. Knoop, H., Zilliges, Y., Lockau, W. & Steuer, R. The metabolic network of *Synechocystis* sp. PCC 6803: Systemic properties of autotrophic growth. *Plant Physiol.* **154**, 410–422 (2010).
26. Orth, J. D., Thiele, I. & Palsson, B. Ø. What is flux balance analysis? *Nat. Biotechnol.* **28**, 245–248 (2010).
27. Englund, E., Shabestary, K., Hudson, E. P. & Lindberg, P. Systematic overexpression study to find target enzymes enhancing production of terpenes in *Synechocystis* PCC 6803, using isoprene as a model compound. *Metab. Eng.* **49**, 164–177 (2018).
28. Anfelt, J. et al. Genetic and nutrient modulation of acetyl-CoA levels in *Synechocystis* for n-butanol production. *Microb. Cell Fact.* **14**, 167 (2015).
29. Yoshikawa, K., Toya, Y. & Shimizu, H. Metabolic engineering of *Synechocystis* sp. PCC 6803 for enhanced ethanol production based on flux balance analysis. *Bioproc. Biosyst. Eng.* **40**, 791–796 (2017).
30. Wilson, J., Gering, S., Pinard, J., Lucas, R. & Briggs, B. R. Bio-production of gaseous alkenes: ethylene, isoprene, isobutene. *Biotechnol. Biofuels* **11**, 234 (2018).
31. Friedlingstein, P. et al. Global Carbon Budget 2020. *Earth Syst. Sci. Data* **12**, 3269–3340 (2020).
32. Rana, A. et al. A combined photobiological–photochemical route to C10 cycloalkane jet fuels from carbon dioxide via isoprene. *Green. Chem.* **24**, 9602–9619 (2022).
33. Kang, M.-K. & Nielsen, J. Biobased production of alkanes and alkenes through metabolic engineering of microorganisms. *J. Ind. Microbiol. Biotechnol.* **44**, 613–622 (2017).
34. Lindberg, P., Park, S. & Melis, A. Engineering a platform for photosynthetic isoprene production in cyanobacteria, using *Synechocystis* as the model organism. *Metab. Eng.* **12**, 70–79 (2010).
35. Mustila, H., Kugler, A. & Stensjö, K. Isobutene production in *Synechocystis* sp. PCC 6803 by introducing α-ketoisocaproate dioxygenase from *Rattus norvegicus*. *Metab. Eng. Commun.* **12**, e00163 (2021).
36. Ungerer, J. et al. Sustained photosynthetic conversion of CO_2 to ethylene in recombinant cyanobacterium *Synechocystis* 6803. *Energy Environ. Sci.* **5**, 8998 (2012).
37. Yunus, I. S. et al. Synthetic metabolic pathways for conversion of CO_2 into secreted short-to medium-chain hydrocarbons using cyanobacteria. *Metab. Eng.* **72**, 14–23 (2022).
38. Edwards, J. S., Ramakrishna, R. & Palsson, B. O. Characterizing the metabolic phenotype: A phenotype phase plane analysis. *Biotechnol. Bioeng.* **77**, 27–36 (2002).
39. Chung, B. K. S. & Lee, D.-Y. Flux-sum analysis: a metabolite-centric approach for understanding the metabolic network. *BMC Syst. Biol.* **3**, 117 (2009).
40. Kim, P.-J. et al. Metabolite essentiality elucidates robustness of *Escherichia coli* metabolism. *Proc. Natl Acad. Sci.* **104**, 13638–13642 (2007).
41. Erdrich, P., Knoop, H., Steuer, R. & Klamt, S. Cyanobacterial biofuels: new insights and strain design strategies revealed by computational modeling. *Microb. Cell Fact.* **13**, 128 (2014).
42. Boecker, S., Zahoor, A., Schramm, T., Link, H. & Klamt, S. Broadening the scope of enforced ATP wasting as a tool for metabolic engineering in *Escherichia coli*. *Biotechnol. J.* **14**, 1800438 (2019).
43. Brinkmann-Chen, S. et al. General approach to reversing ketol-acid reductoisomerase cofactor dependence from NADPH to NADH. *Proc. Natl Acad. Sci.* **110**, 10946–10951 (2013).
44. Kämäräinen, J. et al. Physiological tolerance and stoichiometric potential of cyanobacteria for hydrocarbon fuel production. *J. Biotechnol.* **162**, 67–74 (2012).
45. Knoop, H. & Steuer, R. A computational analysis of stoichiometric constraints and trade-offs in cyanobacterial biofuel production. *Front. Bioeng. Biotechnol.* **3**, 47 (2015).
46. Antoniewicz, M. R. A guide to metabolic flux analysis in metabolic engineering: Methods, tools and applications. *Metab. Eng.* **63**, 2–12 (2021).
47. Cooley, J. W. & Vermaas, W. F. J. Succinate dehydrogenase and other respiratory pathways in thylakoid membranes of *Synechocystis* sp. strain PCC 6803: Capacity comparisons and physiological function. *J. Bacteriol.* **183**, 4251–4258 (2001).
48. Agarwal, R., Ortleb, S., Sainis, J. K. & Melzer, M. Immunoelectron microscopy for locating calvin cycle enzymes in the thylakoids of *Synechocystis* 6803. *Mol. Plant* **2**, 32–42 (2009).
49. Maruyama, M. et al. Time-resolved analysis of short term metabolic adaptation at dark transition in *Synechocystis* sp. PCC 6803. *J. Biosci. Bioeng.* **128**, 424–428 (2019).
50. Johansson, N., Quehl, P., Norbeck, J. & Larsson, C. Identification of factors for improved ethylene production via the ethylene forming enzyme in chemostat cultures of *Saccharomyces cerevisiae*. *Microb. Cell Fact.* **12**, 89 (2013).
51. Nishiguchi, H. et al. Transomics data-driven, ensemble kinetic modeling for system-level understanding and engineering of the cyanobacteria central metabolism. *Metab. Eng.* **52**, 273–283 (2019).
52. Flores, E. Studies on the regulation of arginine metabolism in cyanobacteria should include mixotrophic conditions. *MBio* **12**, e0143321 (2021).
53. Ueda, K. et al. Metabolic flux of the oxidative pentose phosphate pathway under low light conditions in *Synechocystis* sp. PCC 6803. *J. Biosci. Bioeng.* **126**, 38–43 (2018).

54. Xiong, W. et al. The plasticity of cyanobacterial metabolism supports direct CO_2 conversion to ethylene. *Nat. Plants* **1**, 15053 (2015).
55. Ishikawa, Y. et al. One of the NAD kinases, sll1415, is required for the glucose metabolism of *Synechocystis* sp. PCC 6803. *Plant J.* **98**, 654–666 (2019).
56. Ishikawa, Y. et al. The NAD Kinase Slr0400 Functions as a growth repressor in *Synechocystis* sp. PCC 6803. *Plant Cell Physiol.* **62**, 668–677 (2021).
57. Forti, G., Furia, A., Bombelli, P. & Finazzi, G. In vivo changes of the oxidation-reduction state of NADP and of the ATP/ADP cellular ratio linked to the photosynthetic activity in *Chlamydomonas reinhardtii*. *Plant Physiol.* **132**, 1464–1474 (2003).
58. Cano, M. et al. Glycogen synthesis and metabolite overflow contribute to energy balancing in cyanobacteria. *Cell Rep.* **23**, 667–672 (2018).
59. Holland, S. C. et al. Impacts of genetically engineered alterations in carbon sink pathways on photosynthetic performance. *Algal Res.* **20**, 87–99 (2016).
60. Makowka, A. et al. Glycolytic shunts replenish the Calvin–Benson–Bassham cycle as anaplerotic reactions in cyanobacteria. *Mol. Plant* **13**, 471–482 (2020).
61. Veetil, V. P., Angermayr, S. A. & Hellingwerf, K. J. Ethylene production with engineered *Synechocystis* sp PCC 6803 strains. *Microb. Cell Fact.* **16**, 34 (2017).
62. Davies, F. K., Work, V. H., Beliaev, A. S. & Posewitz, M. C. Engineering limonene and bisabolene production in wild type and a glycogen-deficient mutant of *Synechococcus* sp. PCC 7002. *Front. Bioeng. Biotechnol.* **2**, 21 (2014).
63. Bricker, T. M. et al. The malic enzyme is required for optimal photoautotrophic growth of *Synechocystis* sp. strain PCC 6803 under continuous light but not under a diurnal light regimen. *J. Bacteriol.* **186**, 8144–8148 (2004).
64. Jazmin, L. J. et al. Isotopically nonstationary ^{13}C flux analysis of cyanobacterial isobutyraldehyde production. *Metab. Eng.* **42**, 9–18 (2017).
65. Carrer, A. et al. Acetyl-CoA metabolism supports multistep pancreatic tumorigenesis. *Cancer Discov.* **9**, 416–435 (2019).
66. Noor, E., Eden, E., Milo, R. & Alon, U. Central carbon metabolism as a minimal biochemical walk between precursors for biomass and energy. *Mol. Cell* **39**, 809–820 (2010).
67. Xiong, W. et al. Phosphoketolase pathway contributes to carbon metabolism in cyanobacteria. *Nat. Plants* **2**, 15187 (2016).
68. Tedeschi, P. M. et al. Contribution of serine, folate and glycine metabolism to the ATP, NADPH and purine requirements of cancer cells. *Cell Death Dis.* **4**, e877–e877 (2013).
69. Lewis, N. E. et al. Omic data from evolved *E. coli* are consistent with computed optimal growth from genome-scale models. *Mol. Syst. Biol.* **6**, 390 (2010).
70. Ebrahim, A., Lerman, J. A., Palsson, B. O. & Hyduke, D. R. COBRApy: COnstraints-Based Reconstruction and Analysis for Python. *BMC Syst. Biol.* **7**, 74 (2013).
71. Lieven, C. et al. MEMOTE for standardized genome-scale metabolic model testing. *Nat. Biotechnol.* **38**, 272–276 (2020).
72. King, Z. A. et al. Escher: A web application for building, sharing, and embedding data-rich visualizations of biological pathways. *PLOS Comput. Biol.* **11**, e1004321 (2015).
73. King, Z. A. et al. BiGG Models: A platform for integrating, standardizing and sharing genome-scale models. *Nucleic Acids Res.* **44**, D515–D522 (2016).
74. Zhang, S. & Bryant, D. A. The tricarboxylic acid cycle in cyanobacteria. *Science* **334**, 1551–1553 (2011).
75. Steinhauser, D., Fernie, A. R. & Araújo, W. L. Unusual cyanobacterial TCA cycles: not broken just different. *Trends Plant Sci.* **17**, 503–509 (2012).
76. Xiong, W., Brune, D. & Vermaas, W. F. J. The γ-aminobutyric acid shunt contributes to closing the tricarboxylic acid cycle in *Synechocystis* sp. PCC 6803. *Mol. Microbiol.* **93**, 786–796 (2014).
77. Bachhar, A. & Jablonsky, J. A new insight into role of phosphoketolase pathway in *Synechocystis* sp. *PCC 6803. Sci. Rep.* **10**, 22018 (2020).
78. Chen, X. et al. The Entner–Doudoroff pathway is an overlooked glycolytic route in cyanobacteria and plants. *Proc. Natl Acad. Sci.* **113**, 5441–5446 (2016).
79. Klemke, F. et al. Identification of the light-independent phosphoserine pathway as an additional source of serine in the cyanobacterium *Synechocystis* sp. PCC 6803. *Microbiology* **161**, 1050–1060 (2015).
80. Bonner, C. A., Jensen, R. A., Gander, J. E. & Keyhani, N. O. A core catalytic domain of the TyrA protein family: arogenate dehydrogenase from. *Synechocystis. Biochem. J.* **382**, 279–291 (2004).
81. Lea-Smith, D. J., Bombelli, P., Vasudevan, R. & Howe, C. J. Photosynthetic, respiratory and extracellular electron transport pathways in cyanobacteria. *Biochim. Biophys. Acta - Bioenerg.* **1857**, 247–255 (2016).
82. Varma, A., Boesch, B. W. & Palsson, B. O. Stoichiometric interpretation of *Escherichia coli* glucose catabolism under various oxygenation rates. *Appl. Environ. Microbiol.* **59**, 2465–2473 (1993).
83. Stouthamer, A. H. & van Verseveld, H. W. Microbial energetics should be considered in manipulating metabolism for biotechnological purposes. *Trends Biotechnol.* **5**, 149–155 (1987).
84. Yunus, I. S. et al. Synthetic metabolic pathways for photobiological conversion of CO_2 into hydrocarbon fuel. *Metab. Eng.* **49**, 201–211 (2018).
85. Hucka, M. et al. The systems biology markup language (SBML): a medium for representation and exchange of biochemical network models. *Bioinformatics* **19**, 524–531 (2003).
86. Mahadevan, R. & Schilling, C. H. The effects of alternate optimal solutions in constraint-based genome-scale metabolic models. *Metab. Eng.* **5**, 264–276 (2003).
87. Gopalakrishnan, S. & Maranas, C. D. ^{13}C metabolic flux analysis at a genome-scale. *Metab. Eng.* **32**, 12–22 (2015).
88. Schmidt, K. et al. ^{13}C tracer experiments and metabolite balancing for metabolic flux analysis: Comparing two approaches. *Biotechnol. Bioeng.* **58**, 254–257 (1998).
89. Schellenberger, J., Lewis, N. E. & Palsson, B. Ø. Elimination of thermodynamically infeasible loops in steady-state metabolic models. *Biophys. J.* **100**, 544–553 (2011).
90. Young, J. D., Shastri, A. A., Stephanopoulos, G. & Morgan, J. A. Mapping photoautotrophic metabolism with isotopically nonstationary ^{13}C flux analysis. *Metab. Eng.* **13**, 656–665 (2011).
91. Feist, A. M. & Palsson, B. O. The biomass objective function. *Curr. Opin. Microbiol.* **13**, 344–349 (2010).
92. Anfelt, J., Hallström, B., Nielsen, J., Uhlén, M. & Hudson, E. P. Using transcriptomics to improve butanol tolerance of *Synechocystis* sp. strain PCC 6803. *Appl. Environ. Microbiol.* **79**, 7419–7427 (2013).
93. Nilsson, A., Shabestary, K., Brandão, M. & Hudson, E. P. Environmental impacts and limitations of third-generation biobutanol: Life cycle assessment of *n*-butanol produced by genetically engineered cyanobacteria. *J. Ind. Ecol.* **24**, 205–216 (2020).

ACKNOWLEDGEMENTS

This work was supported by Formas—A Swedish Research Council for Sustainable Development" (project no. 2021-01669), Swedish Energy Agency (project no. 44728-1), NordForsk Nordic Center of Excellence 'NordAqua' (project no. 82845) and Carl Tryggers foundation (CTS 20:412). The authors would like to thank Kiyan Shabestary and Pia Lindberg for valuable discussions.

AUTHOR CONTRIBUTIONS

A.K.: Conceptualization, Methodology, Software, Data curation, Investigation, Formal analysis, Validation, Visualization, Writing-Original Draft, Writing-Review & Editing. K.S.: Conceptualization, Supervision, Funding Acquisition, Writing-Review & Editing. All authors read and approved the final version of the paper.

FUNDING

Open access funding provided by Uppsala University.

COMPETING INTERESTS

The authors declare no competing interests.

ADDITIONAL INFORMATION

Supplementary information The online version contains supplementary material available at https://doi.org/10.1038/s41540-023-00307-3.

Correspondence and requests for materials should be addressed to Karin Stensjö.

Reprints and permission information is available at http://www.nature.com/reprints

Publisher's note Springer Nature remains neutral with regard to jurisdictional claims in published maps and institutional affiliations.